Crystallization of a Quasi-Two-Dimensional Granular Fluid

P. M. Reis,* R. A. Ingale, and M. D. Shattuck
Benjamin Levich Institute, The City College of the City University of New York, 140th Street and Convent Avenue, New York, New York 10031, USA
(Received 15 March 2006; published 26 June 2006)

We experimentally investigate the crystallization of a uniformly heated quasi-2D granular fluid as a function of the filling fraction. Our experimental results for the Lindemann melting criterion, the radial distribution function, the bond order parameter, and the statistics of topological changes at the particle level are the same as those found in simulations of equilibrium hard disks. This direct mapping suggests that the study of equilibrium systems can be effectively applied to study nonequilibrium steady states such as those found in our driven and dissipative granular system.

DOI: 10.1103/PhysRevLett.96.258001 PACS numbers: 81.05.Rm, 64.70.Dv, 05.70.Ln, 01.50.Pa

Equilibrium statistical mechanics is generally not applicable to systems far from equilibrium where both energy input and dissipation mechanisms are present, and identifying relevant tools for understanding these systems poses a serious challenge to the scientific community [1]. Granular materials have become a canonical system to explore such ideas since they are inherently dissipative due to interparticle frictional contacts and inelastic collisions. Granular materials also have far reaching practical importance in a number of industries, but often accumulated *ad hoc* knowledge is the only design tool used [2]. The dissipative nature of grains means that any dynamical study requires energy injection, typically involving vibration or shear [3]. An important feature of this class of systems is that the driving and dissipation mechanisms can be made to balance such that a steady state is achieved. Recent investigation of such nonequilibrium steady states has shown that connections with equilibrium statistical mechanics may provide an useful analogy. For example, a single particle on a turbulent air flow has been shown to exhibit equilibriumlike dynamics [4], and the nature of the melting phase transition in two-dimensional granular system is consistent with the Kosterlitz-Thouless-Halperin-Nelson-Young scenario for melting of equilibrium 2D crystals [5].

In our study, we have developed an experimental system to generate a vibrated quasi-two-dimensional granular fluid of stainless steel spheres that is *uniformly heated* (i.e., energy injection is spatially homogeneous). In insets (a) and (b) in Fig. 1, we present two such examples of typical nonequilibrium steady states for filling fractions $\phi = 0.60$ and $\phi = 0.76$, respectively. The first ($\phi = 0.60$) is a disordered dense fluid; there is a high collisional rate and at long times the particles randomly diffuse across the cell. The second ($\phi = 0.76$) is *crystallized* with each sphere packed into a hexagonal array locked by its six neighbors.

In this Letter, we analyze the fluid-to-crystal transition as a function of the filling fraction. The aim of our study is twofold. First, we make a quantitative characterization of the structural changes in the granular layer across this transition using a number of classic measures, namely, the Lindemann criterion for melting, the radial distribution function, and the bond order parameter. Then we apply the novel concept of *shape factor*, recently introduced by Moucka and Nezbeda [6], to measure in detail the topology of the Voronoi cells across the crystallization transition. In parallel, we establish a direct comparison between the behavior of our experimental system and that of simulations of equilibrium hard disks and test the extent to which the above quantities can be used to study a nonequilibrium system such as ours. This comparative part of the study shows that the structural configurations adopted by our granular fluid are identical to hard disks in equilibrium.

Our experimental apparatus is adapted from a geometry introduced by Olafsen and Urbach [7]. We inject energy into a collection of stainless steel spheres (diameter $D = 1.191$ mm) through sinusoidal vertical vibration with

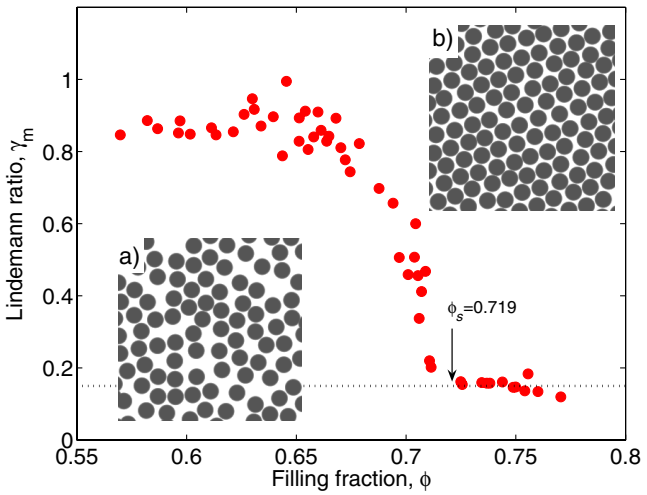

FIG. 1 (color online). Lindemann ratio γ_m vs filling fraction ϕ for a granular layer vibrated at $f = 50$ Hz and $\Gamma = 4$. The dotted horizontal line is located at $\gamma_m = 0.15$. Crystallization occurs at $\phi_s = 0.719$. Insets (a) and (b) are representative experimental frames in the fluid and crystal phases, at $\phi = 0.6$ and $\phi = 0.76$, respectively.

 © 2006 The American Physical Society

frequency f and dimensionless acceleration $\Gamma = A(2\pi f^2/g)$, where A is the amplitude of vibration and g is the gravitational acceleration. The spheres are confined in a fixed volume gap set by a horizontal stainless steel annulus (101.6 mm inner diameter) and sandwiched between two glass plates. The thickness of this annulus is $1.6D$, thus constraining the system to be quasi-2D. The top glass plate is optically flat, but the bottom plate is roughened by sandblasting generating random structures from 50 to 500 μm. Upon vibration, the rough plate homogeneously randomizes the trajectories of the particles. We record the dynamics of the system using high speed photography at 840 Hz and track the particle trajectories in a (15×15) mm^2 central region.

The system is horizontal to minimize gravity-induced effects such as rolling and compaction. We vary the total number of particles in the fixed volume cell over a wide range: from a single particle to an hexagonally packed crystal. We define the *filling fraction* of the granular layer as $\phi = N[D/(2R)]^2$, where N is the total number of spheres, with diameter D in a cell of radius $R = 50.8$ mm. We fix the forcing parameters at $f = 50$ Hz and $\Gamma = 4$ and systematically vary the filling fraction from $0.2 < \phi < 0.8$.

To interpret the qualitative change in behavior between dense fluid and crystalline phases, as ϕ is changed, we first measure the Lindemann ratio. For a wide range of materials, Lindemann found [8] that a solid melts when the vibrational amplitude of its atoms reaches a critical magnitude, typically between 10% and 15%, of the interatomic spacing. The Lindemann ratio in the vicinity of crystallization is $\gamma_m = \sqrt{\langle(\mathbf{r} - \langle\mathbf{r}\rangle)^2\rangle}/L$, where $\mathbf{r}$ is the positional vector of the particles and L is the bond length between (Voronoi) nearest neighbors, corresponding to the average lattice spacing in the crystal phase. In Fig. 1, γ_m is plotted at high values of ϕ. In the range $0.652 < \phi < 0.719$, a sharp drop in γ_m is observed, and, above $\phi > 0.719$, the Lindemann ratio becomes approximately constant at $\gamma_c \sim 0.15$. There the system freezes at $\phi_s = 0.719$ in excellent agreement with the crystallization or *solidus* point, for equilibrium hard disk simulations: $\phi_s^{\mathrm{sim}} = 0.716$ [9].

The Lindemann criterion is empirical and contains little information about structural configurations. For this, we calculate the radial distribution function $g(r)$, which is a standard way of describing the average structure of particulate systems [10]. In Fig. 2(a), we plot curves of $g(r)$ for representative ϕ. For low filling fractions (e.g., $\phi = 0.5$), we observe fluidlike behavior, and $g(r)$ is peaked at $r/D = 1$, 2, and 3, as is commonly seen in hard sphere simulations [10]. At higher ϕ (e.g., $\phi = 0.65$), $g(r)$ develops an additional shoulder below the $r/D = 2$ peak, which at higher densities (e.g., $\phi = 0.7$ and $\phi = 0.72$) evolves into a distinct peak located at $r/D = \sqrt{3}$, signifying hexagonal packing. To each $g(r)$ experimental curve in Fig. 2(a), we have superposed a corresponding (dashed) curve from a Monte Carlo simulation of equilibrium hard disks recently

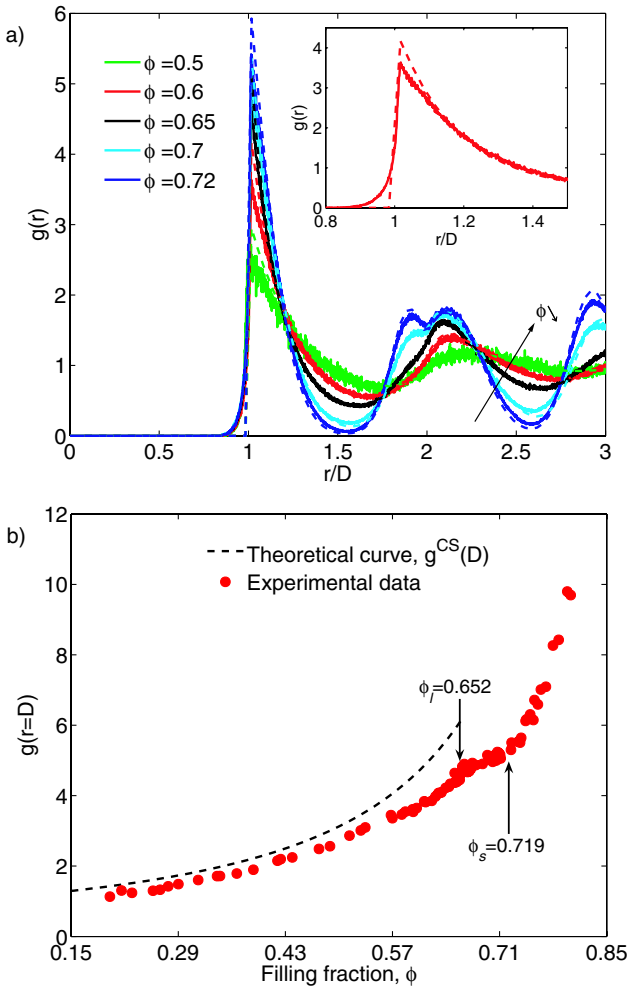

FIG. 2 (color online). (a) Experimental (solid) and numerical (dashed, extracted from Ref. [6]) curves of the radial distribution functions for 5 values of ϕ. The arrow points in the direction of decreasing ϕ. Inset: Section of $g(r)$ curve for $\phi = 0.6$. (b) Radial distribution function at contact, $g(r = D)$ vs the filling fraction. The dashed line corresponds to the theoretical Carnahan-Starling equation [11]. ϕ_l and ϕ_s are the liquidus and solidus points, respectively.

reported by Moucka and Nezbeda [6], for identical values of ϕ. The agreement between the experimental and numerical curves is remarkable, implying that our experimental *nonequilibrium* granular fluid is adopting structural configurations identical to those found in systems of an *equilibrium* hard disk. The only deviations occur near $r/D = 1$, as seen in the inset in Fig. 2(a), for $\phi = 0.60$. This discrepancy is due to the out of plane collisions in our experiments leading to apparent particle overlap in projection, which would not be possible if the system were exactly two-dimensional. The amount of overlap is consistent with our layer thickness of $1.6D$. This deviation is seen in the plot of $g(r = D)$ (i.e., at contact) which corresponds to the absolute maximum of $g(r)$ and is shown in Fig. 2(b). For low filling fractions and up to $\phi \sim 0.57$, $g(D)$ follows the theoretical curve of Carnahan-Starling,

$g^{CS}(D) = [16 - 7\phi]/[16(1-\phi)^2]$, which is usually assumed in the kinetic theory equation of state for granular gases [11], but $g(D)$ is systematically lower than $g^{CS}(D)$ by $\sim$%14. For $\phi > 0.57$, the deviations from $g^{CS}(D)$ increase up to $\phi = 0.652$, where there is a discontinuity in the curve's slope. For $0.652 < \phi < 0.719$, there is a period of slower growth of $g(D)$ with ϕ. This is consistent with the scenario of the existence of a fluid phase ($\phi < 0.652$), an intermediate or transition phase ($0.652 < \phi < 0.719$), and a crystal phase ($\phi > 0.719$). We have performed a parametric study where we varied f and Γ and found that the structure of the granular fluid remained unchanged, as measured by $g(r)$. This is what one would expect for hard spheres where temperature is not a relevant parameter.

In addition to the development of correlations in the particle positions, angular correlations also arise as ϕ is increased [12]. We measure these using the (global) bond-orientational order parameter $\psi_6^{\text{global}} = |1/M \sum_{i=1}^{M} 1/N_i \sum_{j=1}^{N_i} e^{i6\theta_{ij}}|$, where M is the number of particles in the observation window, θ_{ij} is the angle between the particles i and j and an arbitrary but fixed reference axis, and N_i is the number of nearest neighbors of particle i, found using the Voronoi construction [13]. In Fig. 3, we plot the dependence of ψ_6^{global} on ϕ. The value of the bond-orientational order parameter tends to unity in the crystal phase, but $\psi_6^{\text{global}} \ll 1$ for a disordered phase.

As with $g(D)$, three different regions with the same *phase boundaries* $\phi_l = 0.652$ (liquidus point) and $\phi_s = 0.719$ (solidus point) can be identified in Fig. 3 based on the slope of $\psi_6(\phi)$. The observed behavior is consistent with the two-step continuous phase transition observed during equilibrium 2D crystallization [12], where the first transition transforms the isotropic fluid phase into an hexatic phase with long range orientational ordering but no positional ordering, and the second transforms the hexatic phase into a crystal with both long range orientational and positional order.

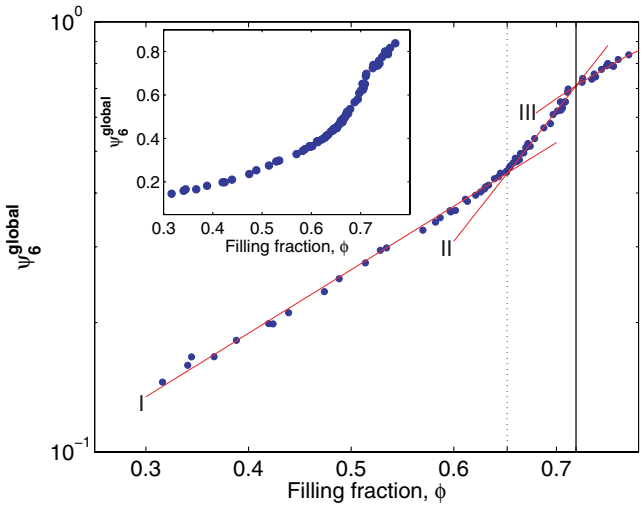

FIG. 3 (color online). Semilogarithmic plot of the bond-orientational order parameter ψ_6. The first two lines, I and II, are least squares fits of the form $\psi \sim \exp[A\phi]$, and line III is a linear fit of the form $\psi \sim A\phi$. The dashed and solid vertical lines are located at $\phi_l = 0.652$ and $\phi_s = 0.719$, respectively. Inset: Linear version of the plot.

Moucka and Nezbeda [6] have recently introduced the concept of *shape factor* ζ, which is a sensitive measure to further quantify structural changes in the fluid-to-crystal transition in 2D. ζ is defined at the particle level, by employing Voronoi tessellation, as $\zeta_i = C_i^2/4\pi S_i$, where S_i is the surface area and C_i the perimeter of the Voronoi cell of the ith particle. For circles $\zeta = 1$, and $\zeta > 1$ for all other shapes [$\zeta = 4/\pi \sim 1.273$ for squares, $\zeta = \pi/5\tan(\pi/5) \sim 1.156$ for regular pentagons, and $\zeta = 6/\sqrt{3\pi^2} \sim 1.103$ for regular hexagons]. Therefore, ζ is a quantifier of the topology of the Voronoi cells associated with the individual particles.

In Fig. 4(a), we present a surface plot of the distribution of shape factor $P(\zeta, \phi)$, and vertical cross sections of $P(\zeta, \phi)$ for fixed ϕ are presented in Fig. 4(b). We superpose numerical (dashed lines) data of Monte Carlo calculations of equilibrium hard disks [6], for the same values of ϕ, and find that our experimental results are in excellent agreement with the numerical simulations. At low ϕ, $P(\zeta)$ exhibits a broad and flat maximum; the particles are randomly distributed and no specific type of cells are formed. As ϕ is increased, $P(\zeta)$ becomes increasingly localized around the maximum, which progressively moves towards lower values of ζ. Eventually, for $\phi > 0.65$ the distribution becomes bimodal and a distinct second maximum appears. In the vicinity of the crystallization point $\phi_s = 0.719$, the original maximum for high ζ values disappears while the low ζ maximum rises sharply (centered at $\zeta \approx 1.1$, the value for regular hexagons). Figure 4(a) clearly shows the existence of two distinct classes of shapes.

To quantify these classes, we follow the classification scheme of the Voronoi cells proposed by Moucka and Nezbeda. An important point to note is that the location of the minimum of $P(\zeta)$, where it exists, is only marginally dependent on ϕ, and we set $\zeta_{\min} = 1.159$. Class A consists of particles with $\zeta < \zeta_{\min}$. Class B particles have $\zeta_{\min} < \zeta < \zeta_u$, and class C have $\zeta > \zeta_u$, where $\zeta_u = 1.25$. The upper bound ζ_u is set such that, at the filling fraction for which both maxima of $P(\zeta)$ have equal heights ($\phi \approx 0.65$), the number of particles in classes A and B are the same. We plot the boundaries of cell classes on the surface plot of $P(\zeta, \phi)$ in Fig. 4(a).

In Fig. 4(c), we present the ϕ dependence of the fraction of particles belonging to each of the classes A, B, and C. The nature of the previously mentioned special filling fraction values of ϕ_l and ϕ_s, which separate the disordered liquid, the intermediate or transition phase, and the crystal phases, becomes clear under this classification. $\phi_l = 0.652$ is the point at which class A and class B occur in the same proportions (the fraction of class C is negligible at this point). $\phi_s = 0.719$ is the point for which the fraction

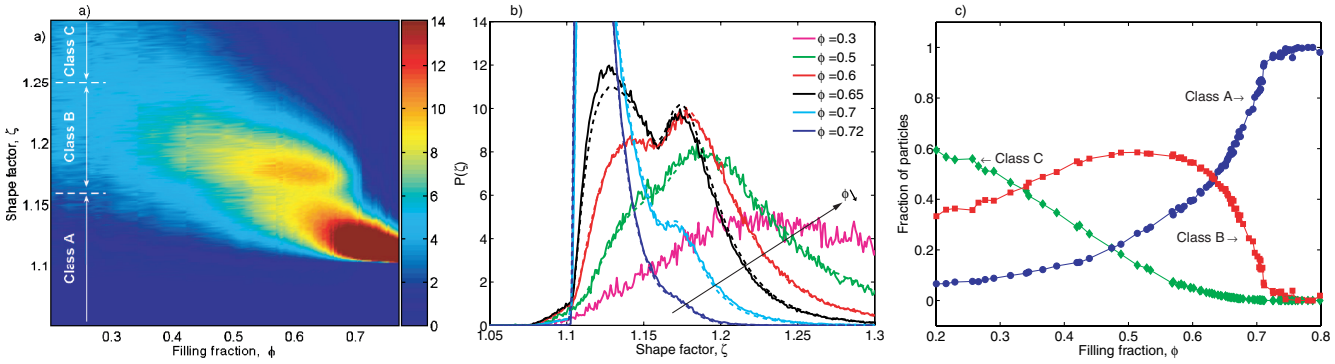

FIG. 4 (color online). (a) Surface plot for the probability distribution functions of shape factor $P(\zeta, \phi)$. The value of $P(\zeta, \phi)$ is given by the adjacent color bar. The two horizontal dashed lines located at $\zeta = 1.159$ and $\zeta = 1.25$ are the boundaries of classes A, B, and C of the Voronoi cells, as defined in the text. (b) Experimental (solid line) and numerical (dashed line, extracted from Ref. [6]) vertical cross sections of the $P(\zeta, \phi)$ distribution along 5 values of ϕ. The arrow points in the direction of decreasing ϕ. (c) Fraction of particles in the A, B, and C classes, as defined in the text, as a function of the filling fraction.

of class B has drastically dropped (but is not strictly zero); the granular layer consists almost entirely of particle whose Voronoi cells are regular hexagons and crystallization occurs. This small but finite value of class B accounts for the existence of dislocations or disclinations, the amount of which decreases with increasing ϕ, as studied in detail by Olafsen and Urbach [5]. It remains to be shown whether the intermediate phase between ϕ_l and ϕ_s is simply a coexistence region as suggested by the leverlike dependence of the fractions of classes A and B, or, instead, it is an hexatic phase with algebraically decaying orientational order [5]. One would need to perform the experiments with a considerably larger imaging window to have sufficient spacial extension to properly test such scalings.

In conclusion, we have reported detailed experimental measures of structural changes during the crystallization transition in a homogeneously heated granular fluid. Our results are in excellent quantitative agreement with Monte Carlo simulations for the crystallization of equilibrium hard disks. It is surprising that the particles in our granular layer adopt equilibriumlike structural configurations even though the system is both driven and dissipative, i.e., far from equilibrium. We believe that the principal ingredients that allow us to establish such a direct analogy are the homogeneity and uniformity of the energy injection along with the importance of geometrical effects. The equilibrium structural configurations for hard disks are usually determined by an entropy maximization argument [14]. Whether we are able to explain the observed phase transitions in our system with entropiclike arguments similar to those used in hard sphere systems is an important question which arises from our study and needs further investigation.

We thank Ivo Nezbeda for allowing us to reproduce their numerical data presented in Ref. [6]. This work is funded by The National Science Foundation, Math, Physical Sciences Department of Materials Research under the Faculty Early Career Development (CAREER) Program (No. DMR-0134837). P. M. R. was partially funded by the Portuguese Ministry of Science and Technology under the POCTI program.

*Present address: PMMH, Ecole Supérieure de Physique et de Chimie Industrielles, 10 rue Vauquelin, 75231 Paris Cedex 05, France.

[1] D. A. Egolf, Science **287**, 101 (2000).
[2] B. J. Ennis, J. Green, and R. Davies, Part. Technol. **90**, 32 (1994).
[3] F. Melo, P. Umbanhowar, and H. L. Swinney, Phys. Rev. Lett. **72**, 172 (1994); B. Miller, C. O'Hern, and R. P. Behringer, Phys. Rev. Lett. **77**, 3110 (1996).
[4] R. P. Ojha, P.-A. Lemieux, P. K. Dixon, A. J. Liu, and D. J. Durian, Nature (London) **427**, 521 (2004).
[5] J. S. Olafsen and J. S. Urbach, Phys. Rev. Lett. **95**, 098002 (2005).
[6] F. Moucka and I. Nezbeda, Phys. Rev. Lett. **94**, 040601 (2005).
[7] J. S. Olafsen and J. S. Urbach, Phys. Rev. E **60**, R2468 (1999); A. Prevost, D. A. Egolf, and J. S. Urbach, Phys. Rev. Lett. **89**, 084301 (2002).
[8] F. A. Lindemann, Phys. Z. **11**, 609 (1910).
[9] B. J. Alder and T. E. Wainwright, Phys. Rev. **127**, 359 (1962); A. C. Mitus, H. Weber, and D. Marx, Phys. Rev. E **55**, 6855 (1997).
[10] J. D. Bernal, Proc. R. Soc. A **280**, 299 (1964); P. M. Chaikin, *Principles of Condensed Matter Physics* (Cambridge University Press, Cambridge, England, 1995).
[11] N. F. Carnahan and K. E. Starling, J. Chem. Phys. **51**, 635 (1969).
[12] D. R. Nelson and B. I. Halperin, Phys. Rev. B **19**, 2457 (1979); A. Jaster, Phys. Rev. E **59**, 2594 (1999).
[13] D. P. Fraser, M. J. Zuckermann, and O. G. Mouritsen, Phys. Rev. A **42**, 3186 (1990).
[14] H. Kawamura, Prog. Theor. Phys. **61**, 1584 (1979).